Particle image velocimetry (PIV) tracking of flow of foamed gypsum slurry under a roller

Kim, Yong Il; Podstawski, David; Sanchez, Caesar; Westerweel, Jerry; Yarin, Alexander L.

DOI
10.1007/s00348-025-04076-z

Publication date
2025

Document Version
Final published version

Published in
Experiments in Fluids

Citation (APA)
Kim, Y. I., Podstawski, D., Sanchez, C., Westerweel, J., & Yarin, A. L. (2025). Particle image velocimetry (PIV) tracking of flow of foamed gypsum slurry under a roller. *Experiments in Fluids*, *66*(8), Article 149. https://doi.org/10.1007/s00348-025-04076-z

Experiments in Fluids (2025) 66:149
https://doi.org/10.1007/s00348-025-04076-z

RESEARCH ARTICLE

Particle image velocimetry (PIV) tracking of flow of foamed gypsum slurry under a roller

Yong Il Kim[1] · David Podstawski[1] · Caesar Sanchez[1] · Jerry Westerweel[2] · Alexander L. Yarin[1]

Received: 15 October 2024 / Revised: 28 June 2025 / Accepted: 30 June 2025

Abstract
Measurement of three-dimensional velocity field of an opaque material (foamed gypsum slurry) flowing under a roller is explored using a PIV surface-tracking technique employoing two types of software. The foamed slurry was deposited on a moving belt pulling it under a rotating roller. The case of the water-to-stucco ratio (WSR) of 75 was studied at 0.19 wt%, and 1.86 wt% of foam added. The cases of roller co-rotation with the belt, no rotation, and counter-rotation were explored. The effect of the added foam on widening of the slurry layer on a roller was also studied. Particle Image Velocimetry (PIV) was used to measure the surface velocity flow field in both top and side views. A significant rejection flow of slurry before the roller was observed in some cases, with its severity varying with the roller's rotating direction, its angular speed, as well as the foam content. One of the main aims of the present work is in the comparison of two PIV software: PIVlab (Matlab source, Germany) and PIVware (provided by TUDelft).

1 Introduction

Detailed studies of flow fields of opaque soft materials such as paper pulp (Brazinsky et al. 1970), cosmetics products (Kusakari et al. 2003), biomedical materials (Ivens et al. 2001; Loeffel et al. 2008), food products (Bourne 2002), and construction materials (Raucci et al. 2018; Li and Ren 2011) are scarce, in spite of their industrial importance and unexpected and fascinating fluid mechanical phenomena. Such a widely used construction material as gypsum slurry, which is in focus in the present work, is a multi-phase material, which is mainly composed of solid particles (gypsum stucco) and water, as well as some starch, fibers and foaming agents. Gypsum–water slurries have been extensively studied and are known to exhibit non-Newtonian characteristics, such as shear thinning and a notable yield stress (Sinha-Ray et al. 2011). Many researchers have successfully employed such rheological constitutive equations as the Ostwald-de Waele power law fluid model (Sinha-Ray et al. 2011), the Herschel–Bulkley model (Liu et al. 2018), the Sisko model (Turian et al. 1997) and the Casson model (Sadeghi et al. 2023) to describe their rheological behavior at different shear rates. The yield stress arises from particle–particle interactions and the hydration-induced structural buildup, while the shear-thinning behavior reflects the progressive breakdown of these interactions at higher shear rates.

It should be emphasized that modern gypsum slurry formulations often incorporate various additives, including foaming agents, fibers and starch aimed at enhancing the material's mechanical, thermal, and acoustic properties and processability (Dannessa et al. 2018). The incorporation of bubbles due to the foaming agents facilitates formation of foamed gypsum, which can further complicate its rheology, altering the viscous and elastic responses, as well as potentially lowering the effective density. Despite the utmost industrial importance of such foamed gypsum slurries, there is relatively scarce published data on the effect of bubbles on the slurry's behavior. In the present work, we address this gap by investigating the flow of foam-laden gypsum slurries under a rotating roller used to deposit a thin slurry layer onto a moving substrate (paper). The effects of the bubble content and the rotation speed of the roller are in focus. It should be emphasized that the presence of foam and entrapped bubbles

Yong Il Kim and David Podstawski contributed equally to this work.

✉ Alexander L. Yarin
ayarin@uic.edu

[1] Department of Mechanical and Industrial Engineering, University of Illinois at Chicago, 842 W. Taylor St., Chicago, IL 60607-7022, USA

[2] Laboratory for Aero and Hydrodynamics, Delft University of Technology, Mekelweg 2, 2628 CD Delft, The Netherlands

Published online: 18 July 2025

make gypsum slurry a shear-thinning (pseudoplastic,) highly compressible material with the speed of sound of the order of only 20 m/s (Sinha-Ray et al. 2011; Plog and Yarin 2023; Pelot et al. 2016).

Gypsum slurries are used to form wallboard by a rotating roller spreading slurry over a moving paper substrate (cf. Fig. 1). This type of flow is in focus in the present work. The observed flow characteristics are expected to exhibit lubrication-like or journal-bearing-like behavior (Pelot et al. 2016, 2013), albeit with an important spanwise spreading due to the unconstrained flow geometry in the spanwise direction. Following the terminology accepted in the literature, here the journal bearing flow implies a flow entrained into a narrow confinement accompanied by the formation of a high-pressure zone within the narrow gap due to significant viscous resistance.

Application of Particle Image Velocimetry (PIV) to opaque materials is mostly uncharted territory (Poelma 2020; Adrian and Westerweel 2011; Xu et al. 2020). Digital Image Correlation (DIC), on the other hand, is commonly used for analyzing deformation in opaque, solid materials, but is unsuitable for analyzing fluid flows. (Zhang et al. 2019) To overcome the inability of such optical methods as PIV to observe the flow field in the bulk of the opaque materials, X-rays or ultrasonic waves were employed (Zheng et al. 2006; Lee et al. 2009). Surrogate, transparent model fluids, were also used instead of such opaque materials, as concrete (Auernhammer et al. 2020). For such rheologically complex materials as foamed gypsum slurries, it is practically impossible to find an appropriate transparent surrogate material. Accordingly, here an attractive approach would be

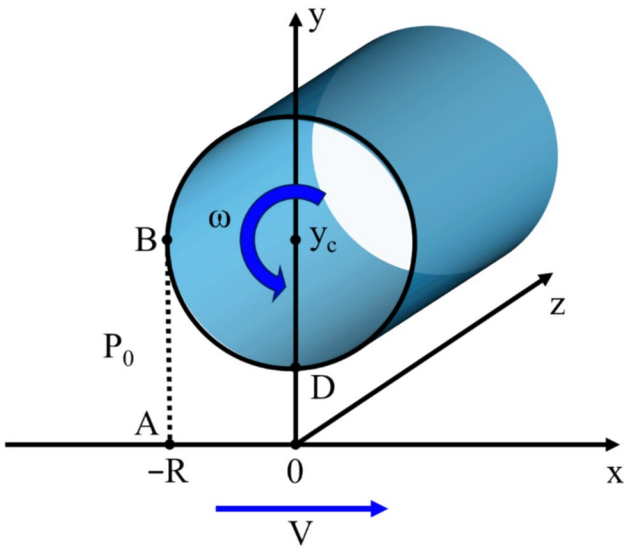

Fig. 1 Schematic of a belt moving with velocity V and carrying gypsum slurry layer into an narrow gap under a roller of radius R rotating with the angular speed ω

dispersing seeding tracer particles and tracking their motion using PIV (Le et al. 2015). The results that could be obtained in the framework of such an approach and their limitations and drawbacks are in focus of the present work. As tracers, coffee particles are used.

In the recent accompanied paper (Kim et al. 2025) published by this group it was shown that the theory developed in Ref. Plog and Yarin (2023) for slurry without foam accurately predicts the lateral spreading in the corresponding case. In contrast, the current work focuses on foamed slurry, which introduces additional complexities in flow behavior. One of the objectives of the present work is to experimentally investigate these new flow features and to contrast the findings with those without foam.

2 Materials and methods

2.1 Materials

The gypsum slurries were prepared by mixing four materials: gypsum stucco ($CaSO_4$, Sheetrock® all-purpose joint compound), a heat-resistant accelerator (a salt which promotes crystallization, HRA, gypsum plaster accelerator), a retarder (an acid, which slows down crystallization), and a foaming agent (Steol CS-230, Stepan Company, USA). All these materials were supplied by the United States Gypsum Corporation (USG, USA). In addition, a plastic wrap (Unbleached compostable parchment paper, Reynolds Kitchens, USA) was employed as a belt carrying gypsum slurry toward the roller. Ground-up coffee particles (100% Colombian coffee, Kirkland, Inc., USA) were scattered over gypsum slurry. Those particles visible on the free surface were used as tracer particles for PIV measurements.

2.2 Preparation of foamed gypsum slurries

To obtain a slurry with a water-stucco ratio (WSR) of 75, two mixtures were prepared separately. In the first mixture, 45 g of gypsum stucco was mixed with 0.225 g of the accelerator HRA. Separately, 0.15 g of retarder was dissolved in 33.75 g of deionized water to extend the working time via inhibition of slurry solidification. Then, a certain amount of the foaming agent was added to the retarder-water mixture. The amount of the foaming agent was in the 0.15−1.5 g range (0.19, and 1.86 wt%) to control the air bubble content and thus, the slurry compressibility. Note that the average bubble size sustained by the foaming agent was 0.2 mm in diameter which was 10 times smaller than the gap between the roller and the belt. Then, the two mixtures were blended by a mixer (Magic bullet mini, Homeland Housewares, USA) for 10 s. The slurry was prepared, and then coffee particles were added immediately, right after which the experiment

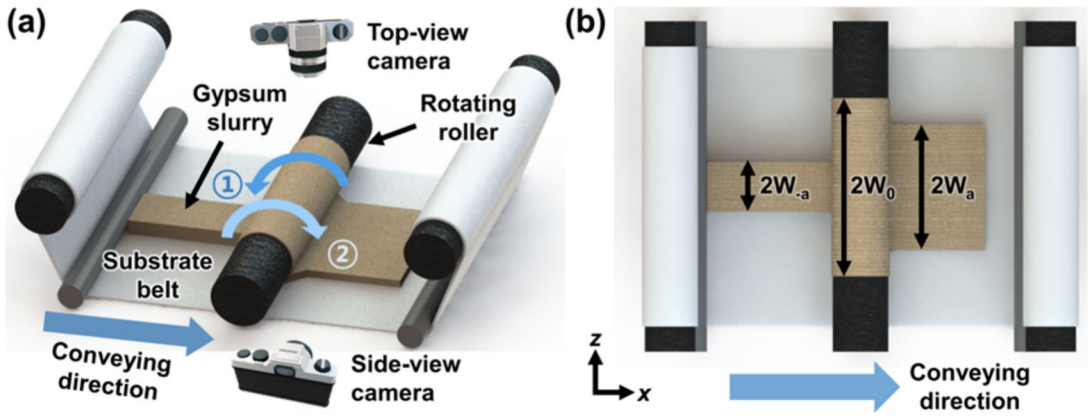

Fig. 2 Experimental setup. **a** Isometric view; **b** top view

was conducted. Note that the rheological behavior of the gypsum slurry used in this study is of the shear-thinning type. The previous work of the present group revealed that this type of slurry (75 WSR without foam) in simple shear follows the power-law (the Ostwald–de Waele) model, with the flow behavior index typically in the n = 0.35 to 0.55 range and the consistency index K varying from 51 to 105 g/cm·s^{2-n} (Sinha-Ray et al. 2011). At high shear rates on the order of 10^3 s^{-1}, as encountered in the roller–substrate gap, the effective viscosity is reduced to approximately 0.1 Pa·s. It should be emphasized that the presence of foam affects the values of n and K depending on the foam content, albeit the rheological behavior still stays that of the shear-thinning type (Dannessa et al. 2018).

2.3 Experimental setup

The experimental setup is sketched in Fig. 2. Two end rollers pulled the paper belt at a constant speed of V = 0.26 m/s. The central forming roller could co-rotate (cf. ① in Fig. 2a) in the belt direction at the angular speeds of 94, 240, or 504 rpm, or not rotate, as well as counter-rotate (cf. ② in Fig. 2a) at the angular speeds of − 94, − 240, or − 504 rpm. The angular speeds of 94, 240, and 504 rpm correspond to the linear velocities of the roller surface of 0.251, 0.641, and 1.345 m/s, respectively. This central roller was made of Delrin (Polyoxymethylene, Dupont, USA) with a size of 5.01 cm (2R, the diameter) × 12 cm (length). The rear-end roller and the other end-roller were powered independently by two motors (DC 12 V, Greartisan, China) and rotated at a fixed speed throughout the experiments. The width of the slurry layer was recorded in a top view by a camera (iPad Pro 3rd Gen., Apple, USA). The width of the gypsum slurry before, on, and behind the central roller was measured (see Figs. 2b and 3).

The slurry-releasing device is sketched in Fig. 4, which also presents its photograph. Gypsum slurry was poured

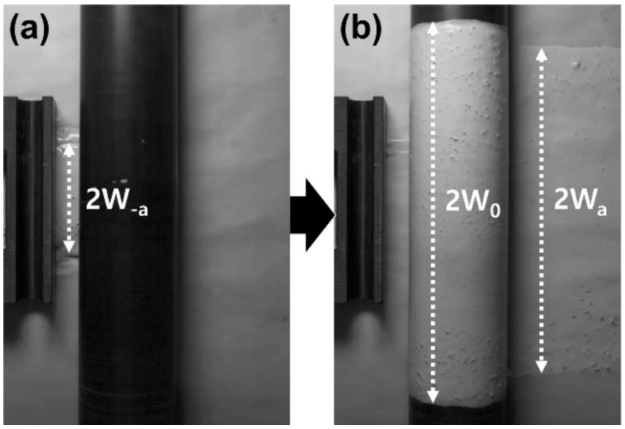

Fig. 3 Photographs of the gypsum slurry layer **a** before entering under the central roller, and **b** on-top and exiting behind the central roller

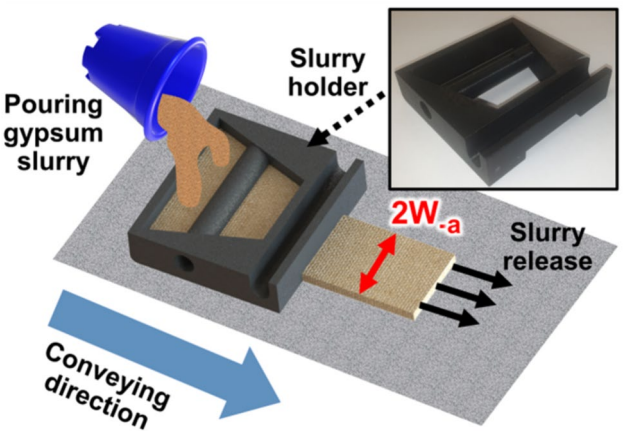

Fig. 4 Release of gypsum slurry onto a conveying belt. Insert: a photo of a slurry holder

into a slurry holder made by a 3D printer. The slurry holder releases gypsum slurry near its bottom as a layer onto a moving belt. The holder has an outlet of 5.1 cm (the width denoted as $2W_{-a}$) in width and 0.65 cm in height. The width and height of the slurry layer were unchanged before an encounter with the central roller. In the present experiment, the slurry was supplied for ~ 3 s in each case. The slurry flow during this time interval could be sub-divided into three distinct stages: (i) the development stage, where the slurry accumulates in front of the roller; (ii) the quasi-steady stage; and (iii) the depletion stage, where the slurry flow is diminishing and ceased. The PIV analysis was performed during the quasi-steady phase and analyzed on a very short time scale compared to the entire length of that phase.

The seeding coffee particles visible at the free surface of the slurry layers were tracked by a Phantom high-speed camera (VEO-E 340L, Vision Research, USA) in the side and top views with a frame rate of 1000 frames per second (fps) and a spatial resolution of 1408 pixel × 1400 pixel area which covers 21.4 mm × 21.3 mm in the physical domain. The density of a coffee particle was close to 0.41 g/cm^3, with sizes in the 100–2000 μm range (Kim et al. 2025). It was observed that while some of these particles dissolved in water (> 1 min), the process was considerably slower than the experimental time frame which was less than 10 s. Note that three repetitions were conducted in each case. The snapshots of the side and top views were analyzed with the help of the two PIV software: PIVlab (Matlab source, Germany) and PIVware (provided by TUDelft). The software was validated by ensuring that key design parameters were met for proper PIV analysis. These include maintaining the image density (the number of particle images per interrogation region) above 10. It also implies that the interrogation region (the subareas into which an image is divided to determine vector displacement between the corresponding images) is adjusted to limit the in-plane displacement to less than 1/4 of the interrogation region. Note also, that the out-of-plane displacement was not a concern, as the coffee particles remained at the surface.

Moreover, in PIVware, correlation averaging (which is particularly suitable for quasi-steady-state flows, such as those in the present experiments) was employed to minimize noise and improve accuracy over instantaneous correlation methods (Meinhart et al. 2000). On the other hand, PIVlab did not employ correlation averaging and was chosen for its ease of use. PIVlab offers a user-friendly interface suitable for those with minimal Matlab or PIV experience, making it easy to upload images, set pixel dimension scales, apply masks, and adjust color map ranges. It also has an active support forum with developer participation. However, it is limited to predefined settings and analysis. In contrast, PIVware requires a more significant Matlab and PIV expertise but offers greater flexibility and options for custom analysis, including advanced methods such as correlation averaging. It is supplemented with helpful tools such as a comprehensive manual with examples and built-in help but has a steeper learning curve. This study compares the results of the experiments on opaque materials conducted with these two types of software. The investigation focuses on the discrepancies between the two methodologies, with and without correlation averaging. The results obtained using PIV are presented in Figure S1 and were used for analysis after additional background removal.

In order to provide a comprehensive explanation of the correlation averaging method employed by PIVware, it is necessary to describe the manner in which this technique accumulates correlation data from a sequence of images, with the objective of constructing the spatial correlation function (Adrian and Westerweel 2011). As Figure S2 illustrates, it first calculates the instantaneous correlation between each of the image pairs in the sequence and then averages them to provide the average displacement for that interrogation region. In the analysis of the side-view images the 3D effect would cause a seed particle visible in the 1st image frame to become invisible in the 2nd image frame. Such particles were excluded from the correlation calculation. As a result, the 2D flow structure was recovered. On the other hand, in Sect. 4 of the accompanying paper (Kim et al. 2025) and in Sect. 3.1.3 of the present work the top-view imaging was used to explore the lateral (3D) component of the flow. Only a combination of the side- and top-view imaging allows one to reconstruct properly all three components of the flow.

For each flow case, a series of 31 consecutive images was utilized. Initially, an appropriate interrogation region (the initial one of 64 pixels × 64 pixels) for each case was determined and the analysis began with examining a portion of the image, termed the region of interest. Subsequently, a smaller region of 32 pixels × 32 pixels was used to enhance resolution. The 64 pixels × 64 pixels region supports a maximum displacement of approximately 16−20 pixels. For cases exhibiting a significant number of points within this range, the initial interrogation region was increased to 128 pixels × 64 pixels. This adjustment provided a more precise depiction of the actual displacement for each case. The correlation averaging method was then applied to the full image using these tailored interrogation regions. Both components of the two-part method incorporated a min−max filter, which enhances image contrast by subtracting the image background. The filtered images were subsequently utilized to compute the displacement vectors within the flow in all cases.

3 Results and discussion

3.1 Experimental results

3.1.1 Measured half-widths of slurry layers

Figure 5 presents the measured width ratios of the slurry layers with different foam contents and different roller rotation speeds corresponding to co-rotation (94−504 rpm, Movie S1), no-rotation (0 rpm, Movie S2), and counter-rotation (− 504 − − 94 rpm, Movie S4). The values of Fig. 5a and b correspond to the ratios W_0/W_{-a} and W_a/W_{-a}, respectively (cf. Figure 3). The values of the ratio W_0/W_{-a} are ~ 13% higher than those of the ratio W_a/W_{-a} in all cases because the slurry layer contracts after leaving the roller as a result of the substrate (the parchment paper) being non-wettable as illustrated in Fig. 6.

A general observation from Fig. 5 is that the width ratio is in average proportional to the roller speed for all foam contents. This trend can be attributed to an increased squeezing effect as the rotational speed increases. In other words, at higher rotational speeds, the squeezing force becomes more significant, generating higher pressure. This facilitates spreading in regions where no physical constraints obstruct the flow. In addition, higher rotation speeds promote shear-thinning phenomenon in the slurry, reducing its shear viscosity and thereby enhancing its flowability (Pelot et al. 2013). This effect ultimately results in a higher width ratio. Increasing the foam content further enhances the width ratio, likely due to an easier lateral spreading at a lower viscosity associated with a higher air content.

In Fig. 5, there are some deviations from the above-mentioned average proportionality. One possible cause of these deviations is the experimental inaccuracies, which may stem from human handling, environmental factors such as relative humidity and temperature fluctuations, or slight inconsistencies in measurements. Another possible explanation is that at extreme rotational speeds (504 or − 504 rpm) an excessive flow entrainment may occur. For instance, at the highest counter-rotation speed (− 504 rpm), splashes from the roller

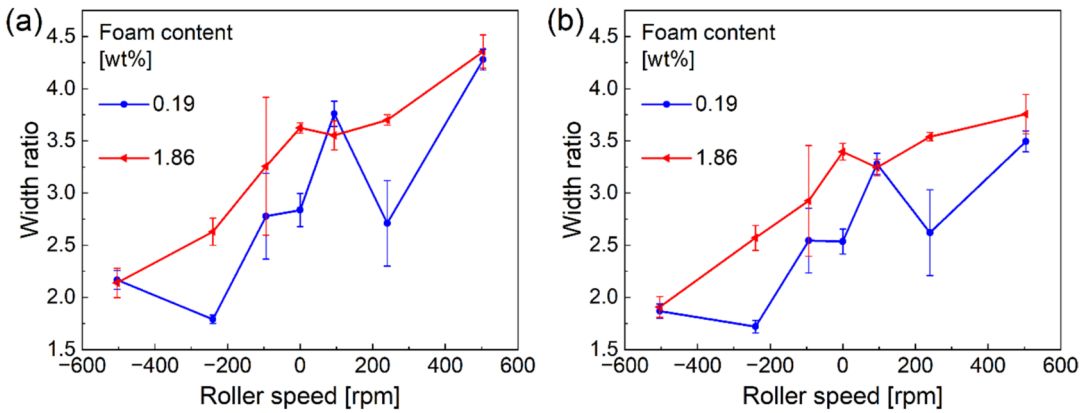

Fig. 5 Width ratios of foamed gypsum slurry layers as functions of the rotation speed of the central roller. **a** Values of W_0/W_{-a}, (with W_0 being the width on the roller) and **b** W_a/W_{-a} (with W_a being the width right behind the roller)

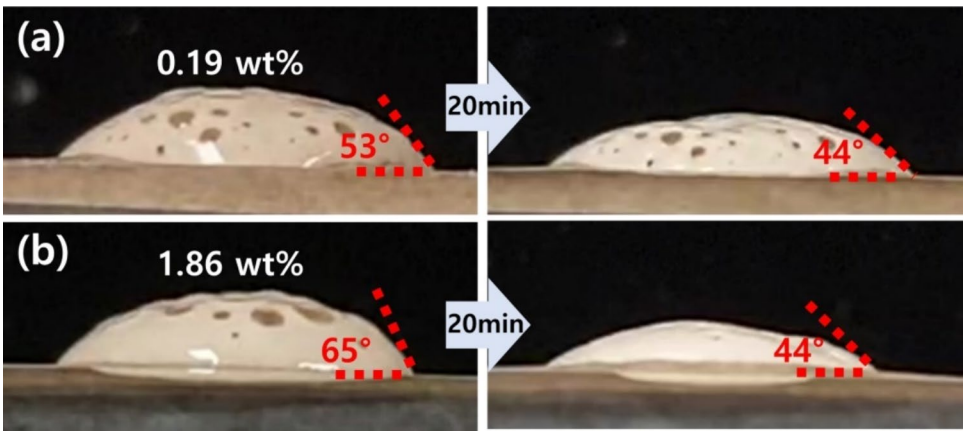

Fig. 6 The apparent contact angle of the gypsum slurry after 20 min with **a** 0.19 wt% of foam, and **b** 1.86 wt% of foam

led to slurry loss in the z-direction beyond the roller width, introducing an experimental discrepancy in the measured values of W (cf. the − 504 rpm case in Movie S4).

Figure 6 illustrates the wettability of the substrate paper by slurry with foam. Note that the black dots on the slurry are air foam. The 0.2 ml foamed slurry droplet was located on parchment paper and recorded for 20 min. Since the initial spreading occurs before significant drying takes place, the overall wetting behavior was primarily governed by surface tension and viscosity. Even though the paper was hydrophobic for pure water and slurry without foam (Kim et al. 2025), a small amount of the foaming agent significantly decreased the contact angle (Fig. 6). Using the pendant droplet method, in the present work it was shown that the surface tension of water was significantly reduced from 71.6 mN/m to 37.08 mN/m and 34.04 mN/m as the surfactant concentration increased from 0 wt% to 0.19 wt% and 1.86 wt%, respectively. In general, foaming agents significantly diminish the surface tension when surfactant concentration increases up to the critical micelle concentration (CMC), whereas above CMC the surface tension reaches a plateau value and does not change anymore with adding surfactants (Sett et al. 2014a; Sankaran et al. 2019). In a sense, the foaming agent acted as a surfactant improving wettability similarly to the so-called superspreaders (Sankaran et al. 2019; Sett et al. 2014b). In addition, the contact angle of the slurry containing the foaming agent decreased significantly in 20 min. Note that the overall volume decrease was due to rapid hydration of gypsum and evaporation of water. Consequently, the contact angle reduction was enhanced as the foaming agent content increased: the 17% and 32% reduction in the contact angle in 20 min at 0.19 and 1.86 wt% content of the foaming agent, respectively.

3.1.2 Side-view PIV measurements of the slurry flow field

Particle image velocimetry (PIV) was used to measure the flow field in the slurry's surface layer carried toward the roller; cf. in Figs. 7, 8 and 9. Note that the visible surface was not flat due to foam-induced three-dimensional structures, and the focus was set at the most optically accessible outermost layer. Therefore, regions lacking velocity vectors may correspond to areas that were out of focus due to this complex three-dimensional surface, rather than an actual absence of flow. Accordingly, regions out of focus may exhibit insufficient visible tracers. In the co-rotation case presented in Figs. 7 and Movie S1 in Supporting Information, the entire slurry layer was entrained through the gap below the roller at any foam content except for the case presented in Fig. 7f, where pressure in the gap increased to such an extent that a discernible reverse flow appeared before the roller. It should be emphasized that the present flow is

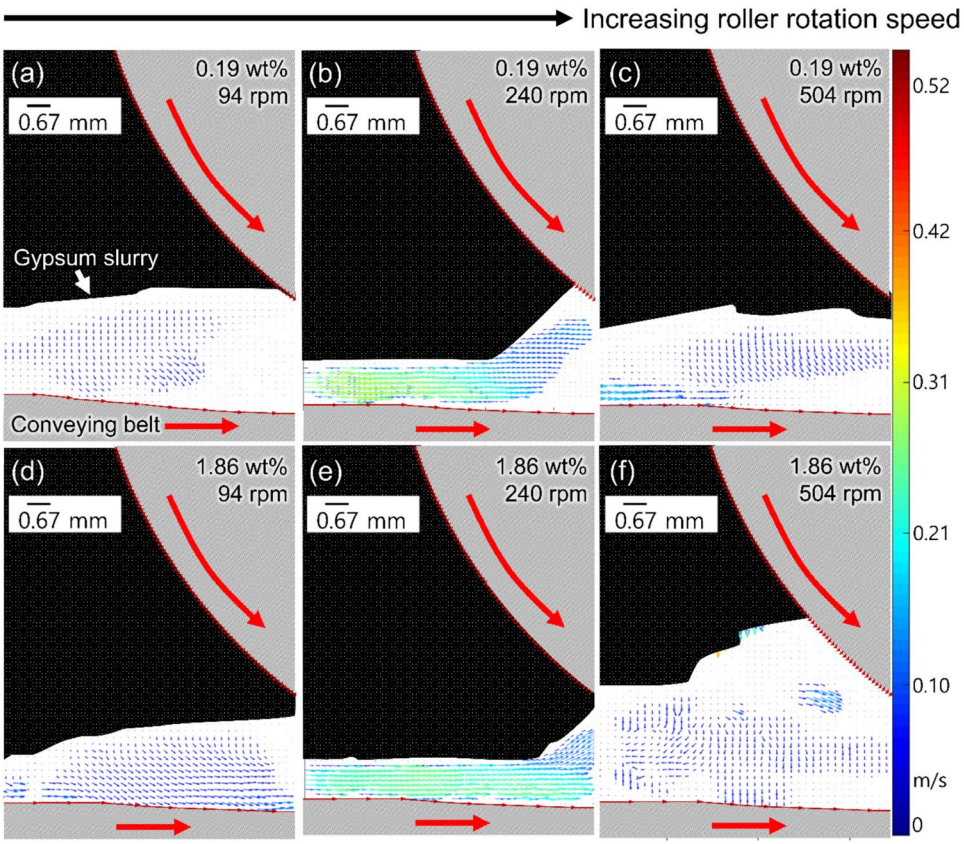

Fig. 7 Vector flow field (the side view) of gypsum slurry entering under a co-rotating roller. Rotation speed: **a**, **d** 94 rpm, **b**, **e** 240 rpm, and **c**, **f** 504 rpm. Foam concentration: **a–c** 0.19 wt%, and **d–f** 1.86 wt%. The color bar characterizes the velocity magnitude. Regions without vectors, blank regions, may not indicate zero flow, but rather areas with insufficient tracer particles where velocity could not be determined

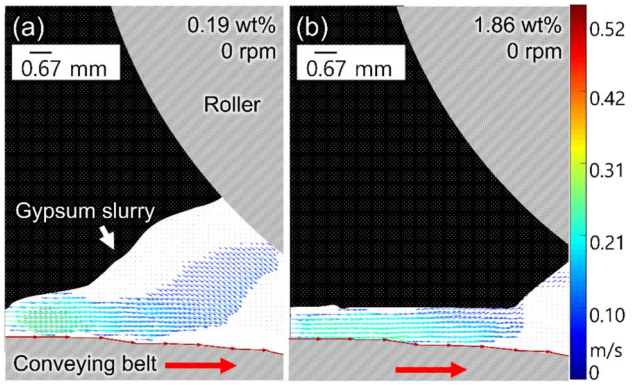

Fig. 8 Vector flow field (the side view) of gypsum slurry entrained under a non-rotating roller. Foam concentration: **a** 0.19 wt%, and **b** 1.86 wt%. The color bar characterizes the velocity magnitude. Regions without vectors, blank regions, may not indicate zero flow, but rather areas with insufficient tracer particles where velocity could not be determined

viscosity-dominated, as the lubricant flow in journal bearings (Sankaran et al. 2019; Schlichting 1979). In such flows a highly viscous fluid driven into a narrow gap by viscous stresses causes a significant increase in pressure (a direct consequence of the momentum balance equation), which is employed to support heavy-loaded axes in rotating journal bearings. Similarly, pressure increases under the roller. In addition, the present results reveal that in all the cases the upper part of the slurry layer moved at a low speed of less than 0.003 m/s before meeting with the roller, whereas the lower part close to the belt moved at a relatively high speed of 0.180 m/s to 0.222 m/s as the main cause of movement is the conveyor belt (see Fig. S3).

Before being entrained under the roller (the leftmost part of the slurry layer was considered), the layers with foam were relatively shallower than those without foam which stems from the enhanced wettability provided by the foaming agent, as illustrated in Fig. 6. Without foam, the thicknesses in the direction normal to the belt were 3.83, 2.96, and 3.54 mm for 94, 240, and 504 rpm, respectively (Kim et al. 2025). As the foam concentrations increased to 0.19 wt%, the thicknesses were 3.77, 2.03, and 3.34 mm for 94, 240, and 504 rpm, respectively, which constitutes a 1.6, 31.4, and 5.6% decrease compared to the corresponding layer thicknesses without foam. With 1.86 wt% foam, the thicknesses were 1.90, 1.76, and 5.04 mm for 94, 240, and 504 rpm, respectively, which constitute a 50.4 and 40.5% decrease, and a 42.4% increase compared to the thicknesses of the corresponding layers without foam.

Accordingly, irrespective of the quantity of foam, the slurry thickness exhibited a notable reduction when the roller speed was increased from 94 to 240 rpm, and exhibited a subsequent increase when the roller speed was increased

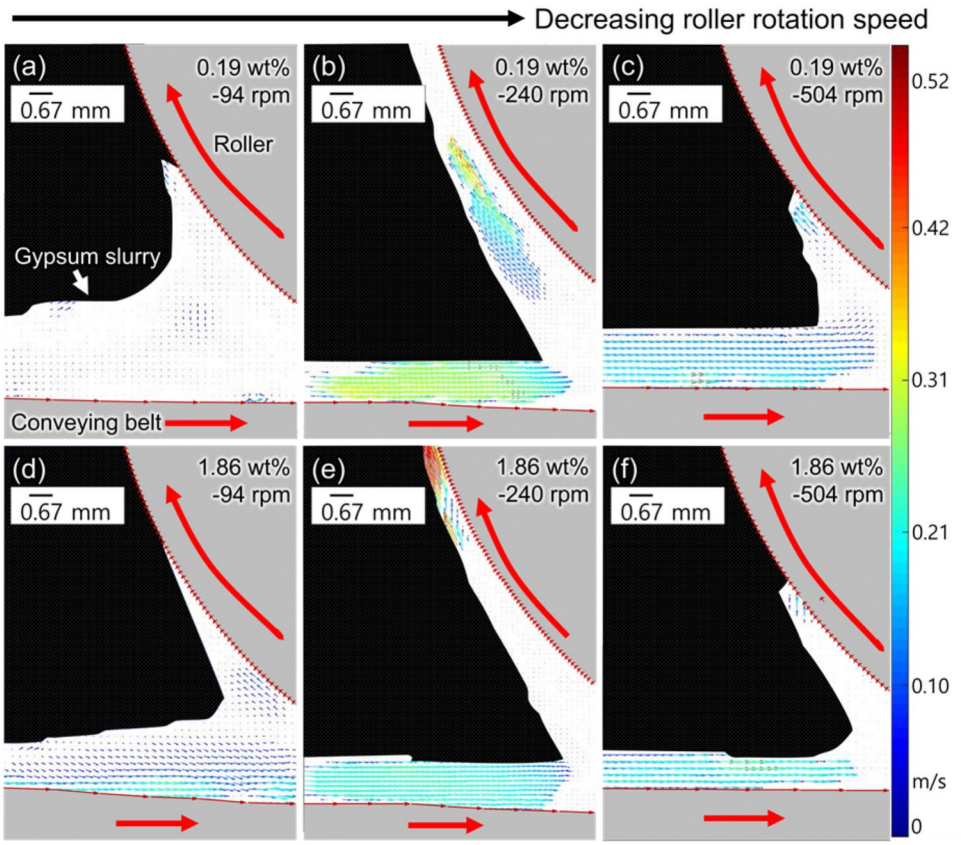

Fig. 9 Vector flow field (the side view) of gypsum slurry entrained under a counter-rotating roller. Rotation speed: **a**, **d** − 94 rpm, **b**, **e** − 240 rpm, and **c**, **f** − 504 rpm. Foam concentration: **a**–**c** 0.19 wt%, and **d**–**f** 1.86 wt%. The color bar characterizes the velocity magnitude. Regions without vectors, blank regions, may not indicate zero flow, but rather areas with insufficient tracer particles where velocity could not be determined

from 240 to 504 rpm. In the lower foam concentration range (0−0.19 wt%), the thickness at 504 rpm was observed to be lower than that at 94 rpm. However, when the foam concentration became higher (1.86 wt%), a significant increase in thickness was noted when the rotation speed increased from 94 to 504 rpm, which was attributed to the substantial back pressure.

Velocity components u in the x-directions, corresponding to the flow fields of Fig. 7 are presented in Fig. S4. Figure S4 reveals no discernible reverse flow in almost all the cases of co-rotating roller. The blue-colored patches corresponding to the reverse flow with $u < 0$ are only pronounced in the case of the highest co-rotation speed with maximum foam content, as illustrated in Fig. S4f. In this case, the adverse pressure gradient becomes sufficient for repelling a light material backward. The reverse flow with the highest foam content and high roller speed is likely to be the result of a combination of factors, including a reduction in density and viscosity caused by the foam. When the adverse pressure gradient is strong enough, the lighter and less viscous foam-filled slurry is unable to resist the backward pressure, resulting in the repulsion of lighter materials.

At a low rotation speed of the roller (as in Fig. S4a and d), the forward flow remained always low irrespective of the foam content. The correlation between the rotation speed of the roller, the foam content, and the velocity component u of the slurry could be recognized at the moderate rotation speed (Fig. S4b and e). The difference in the slurry velocity at the foam content variation is evident at the higher roller speed. Accordingly, one can conclude that a higher foam content with a moderate co-rotation speed enables faster slurry transport.

Figures S5 present the y-component of velocity, v. The vertical flow appears to be influenced by the foam addition in the case of co-rotation. As the foam content increased from 0.19 to 1.86 wt%, both the upward and downward flow components became more pronounced. With an increase in the roller's rotation speed to 240 rpm and 504 rpm, the 'polarization' of the flow is further enhanced, with a higher velocity domain becoming evident.

At 240 rpm, the velocity v scale is approximately 10 times smaller compared to the corresponding velocity component u (see Fig. S4). This suggests that the moderate rotation of the roller facilitates the horizontal transport of the slurry while reducing the layer thickness. As the rotation speed of the roller increases to 504 rpm, the flow 'polarization' becomes even more distinct. The effect of foam is maximized at a foam concentration of 1.86 wt% and a roller speed of 504 rpm. This implies that an excessive roller co-rotation speed, beyond a certain foam concentration, results in a stronger vertical flow rather than horizontal slurry transport.

The case of a non-rotating roller is illustrated in Fig. 8, and Movie S2 in Supporting Information. Before being entrained under the roller (the leftmost parts of the slurry layer in Fig. 8), the slurry with the added foam was relatively shallower than without foam, as it was in the co-rotation cases. Once again, it stems from the wettability differences. Without foam, the layer thickness normal to the belt was 2.65 mm (Kim et al. 2025). It decreased to 2.02 mm and 1.6 mm as the foam content increased to 0.19 and 1.86 wt%, respectively.

The hill-like zone behind the roller in Fig. 8 gradually became less pronounced as the foam content increased, with the maximum thicknesses being 7.05, 7.39, and 4.39 mm for the foam content of 0, 0.19, and 1.86 wt%, respectively. One can conclude that an increase in the foam content might result in a reduction in slurry viscosity and an improvement in flowability. This is likely to lead to a less pronounced formation of the 'hill-like zone'.

Velocity components u in the x-directions, corresponding to the flow fields of Figs. 8 are presented in Figures S6. For a non-rotating roller, the flow of slurry varies depending on the foam content. At 0.19 wt% without roller rotation, the forward flow was observed to be more pronounced than in the 94 rpm case (Figure S4a). This is attributed to the reduction in pressure formed under the roller (Kim et al. 2025). As the foam content increased to 1.86 wt%, the forward flow was more developed with a decreased slurry thickness, which is similar to the case of 240 rpm (Figure S4b). It can be concluded that the effect of foam could intensify slurry transport, similarly to the phenomenon observed with the co-rotating roller at 240 rpm. However, it should be emphasized that, with the exception of the co-rotating speed of 240 rpm, the use of co-rotating rollers has a detrimental impact on the flow of foamed slurry in the x-direction, which is accompanied by a corresponding increase in slurry spreading in the z-direction.

Figures S7 present the y-component of velocity, v. Without roller rotation at low foam concentration, there is a notable development of downward flow, especially right under the roller. While the horizontal velocity component dominates the initial region of the slurry layer (as depicted in Figure S6a), the vertical velocity components become comparable in magnitude as the slurry passes under the roller. At a still higher foam concentration (1.86 wt%, Figure S7b), vertical motion becomes prominent even before reaching the roller, and the previously observed flow under the roller diminishes, indicating a significant change in flow behavior with increasing foam content.

In the case of a counter-rotating roller, the velocity field was also affected by the added foam, as in the co-rotation and no-rotation cases. As the foam content was increased at − 94 rpm, the slurry layers changed, with thicknesses of 3.54 mm and 1.96 mm at the foam contents of 0.19 and 1.86 wt%, respectively. (see Figs. 9a and d) Such a decreasing trend accompanying the addition of foam

was consistent with the other cases illustrated in Figs. 7 and 8. As before, this trend is attributed to differences in wettability.

Without the addition of foam, at the high counter-rotating speed of the roller (− 94 rpm), the released slurry layer height was about 3.74 mm. The addition of foam caused almost no change in the layer height at the same counter-rotation speed (− 94 rpm), with the maximum height being 10.08 mm and 11.04 mm at the foam contents of 0.19 and 1.86 wt%, respectively. (see Fig. 9a and d) However, as the roller's rotation speed decreased to − 240 rpm and − 504 rpm, the influence of foam became more pronounced, with a reduction in the layer thickness. At the lowest speed of − 504 rpm (Figs. 9c and f), the thickness of the slurry layer decreased from 2.57 to 1.70 mm, representing a 33.9% reduction.

In the counter-rotation case, an entrained layer formed on the roller and was carried away regardless of the foam content (Kim et al. 2025). When the rotation speed changed from − 94 to − 240 rpm and further to − 504 rpm (Figs. 9a–c), the height of the entrained layer on the roller changed from 10.08 to 15.62 mm and finally to 8.64 mm, respectively. This suggests that while higher roller speeds initially entrained more slurry, further increases in the speed beyond a certain threshold led to a decrease in the entrained volume. Additionally, as the foam content increased from 0.19 to 1.86 wt%, the heights of the layer on the roller exhibited minimal variation; for example, at − 94 rpm, the heights were 10.08 mm and 11.04 mm, respectively (Fig. 9a and d). Nevertheless, the thickness of the slurry on the roller revealed a substantial reduction, which may be attributed to changes in the wettability of the roller by the slurry.

Velocity components u in the x-directions, corresponding to the flow fields of Fig. 9 are presented in Figure S8. In the counter-rotation case with a low foam concentration and high-speed rotation, the flow velocity remains low throughout the domain, similarly to the low-speed co-rotation case (Figure S4a). Both the forward flow before the roller and the reverse flow on the roller's surface become more prominent as the rotation speed decreases to − 240 rpm. In this scenario, the magnitude of the flows regardless of their direction is greater compared to the other rotations cases (cf. Figure S8b to Figures S4 and S6). This is likely due to a strong backward flow developed at an optimal counter-rotation speed, reinforcing the forward flow. However, when the rotation speed is further changed to − 504 rpm, both the forward and reverse flows diminish.

As the foam content increased from 0.19 to 1.86 wt%, both forward and backward flows became more developed, particularly at the higher counter-rotation speeds (Figure S8). This phenomenon may be attributed to the lighter and less viscous foam-filled slurry, which is more susceptible to the pressure gradients created by the roller's rotation.

Figures S9 present the y-component of velocity, v. In the case of counter-rotation with 0.19 wt% foam and at − 94 rpm, no significant vertical flow was observed, similarly to the results for the x-velocity components in Figure S8a. However, at a moderate rotation speed of − 240 rpm, a relatively strong vertical flow appeared, likely due to the strong entrainment of slurry by the roller at this speed (− 240 rpm). As the roller's speed further decreases, the strong vertical flow diminishes once again. When the foam concentration increases to 1.86 wt%, the vertical flow is reinforced, as seen in Figure S9d–f, though this behavior is not strongly expressed for all conditions.

3.1.3 Lateral flow of gypsum slurry measured in top view

Figure 10 illustrates the velocity field in the z-direction (the lateral direction) recorded in the top view. The data elucidates the effect of foam content on the measured velocity component w. It is noteworthy that a substantial spanwise slurry movement that occurs immediately upon its departure from the holder appears to be a consequence of the pressure build-up caused by the roller. Figure 10b (or Movie S2 in Supporting Information) presents the PIV results for the slow co-rotation case (94 rpm) for different foam contents. As the foam content increased, the lateral spreading of the gypsum slurry decreased (for the 0.19 wt% foam content) and then, was enhanced (for the 1.86 wt% foam content). The average spreading velocity component w decreased from 0.12 to 0.10 m/s in the 0 wt% to 0.19 wt% cases, respectively, which is a ~ 17% decrease. As the foam content increased to 1.86 wt%, the average value of w increased from 0.10 to 0.15 m/s (50% increase). Figure 10c presents the PIV results for the co-rotation case with moderate rotation speed. For the 0.19 wt% foam content, the lateral velocity w increased to ~ 0.13 m/s (by 30%) in comparison to the case without foam (Kim et al. 2025), which could be due to the enhancement of the x-directional slurry transport, as in Fig. 8. The lateral velocity w increased again to ~ 0.15 m/s with the higher co-rotation speed, as illustrated in Fig. 10d, and at the highest foam content. Note that an alternative color arrangement was more appropriate in some cases (see Fig. 10d with the foam content of 1.86 wt% and Movie S2). It should be emphasized that in Fig. 10d (or Movie S2), at the foam content of 1.86 wt%, the PIV results were limited, as the stucco slurry was flung from the roller to the substrate, which hindered the software from being able to analyze the lateral velocity component.

Figure 10e (or Movie S2 in Supporting Information) characterizes the velocity component w in the no-rotation cases. It should be emphasized that the highest lateral velocity component w (~ 0.15 m/s) was observed without foam (Kim et al. 2025), which increased by about 15% as more foaming agent was added.

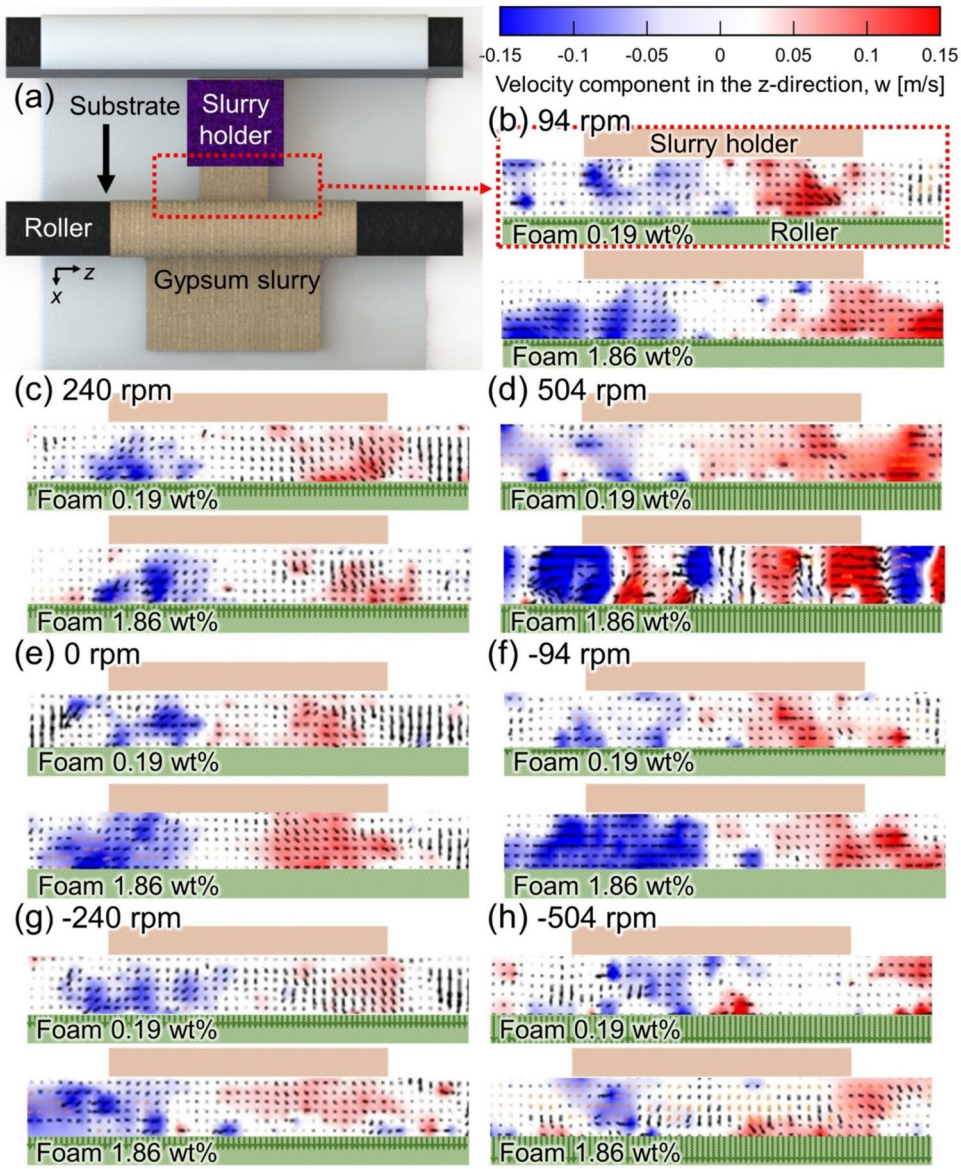

Fig. 10 **a** Schematic of the observation area in the top view. Rotation speed: **b** 94 rpm, **c** 240 rpm, **d** 504 rpm, **e** 0 rpm, **f** − 94 rpm, **g** − 240 rpm, and **h** − 504 rpm. Arrows correspond to the velocity vectors. The color bar represents the velocity component in the *z*-direction, w. Top views suggest that the coffee particles are evenly distributed

Figures 10f–h (or Movie S4 in Supporting Information) present the PIV results for the counter-rotation case with different foam contents. As for the counter-rotation case, also here the lateral velocity w decreased and then increased as foam was added, which is consistent with the results for the layer width W in Fig. 5. In Fig. 10f, the maximum value of the velocity component w increased by 46% from the no-foam case explored in Ref. Kim et al. (2025) to the 0.19 wt% foam content case (− 94 rpm). Also, the maximum velocity component w achieved without foam (~0.10 m/s), is approximately the same as the average value of w in the co-rotation case (Fig. 10b). These values are inconsistent with the results in Fig. 5, where the layer width increase was much higher for the co-rotation case than for the counter-rotation case. Note that the results for the lateral velocity component w discussed here cannot fully characterize the lateral spreading up to the half-width W_0 of Fig. 5, because here only the layer part visible outside the roller is considered (cf. Figure 10a).

3.1.4 Comparison of gypsum slurry flow fields revealed using different software programs

Figures S10−S18 present the PIV results obtained with different software, PIVlab, which was used to verify the previous results from PIVware (see Sect. 3.1.2). Both types of software produced generally consistent outcomes. However, some specific differences were observed. For instance, the flow domain identified by PIVlab was blotchy and contained spurious vectors compared to the results obtained by PIVlab (cf. Figures S10–S18 to Figs. 7, 8 and 9 and Figs. S4 − S9). This is likely due to an insufficient number

of particle images on the surface. While adding more coffee grains could improve particle image density, it might affect foam properties, e.g., promoting bubble coalescence. A more effective approach would be to average the results, either by averaging over multiple measurements, adding image frames, or using correlation averaging. The latter approach, the correlation averaging, used in PIVware seems to be the most effective, as demonstrated in the previous work (Meinhart et al. 2000) based on estimating time-averaged velocity fields. It is worth noting that while correlation averaging is unsuitable for DIC, it is reasonable in the present case dealing with opaque fluids with PIV.

4 Conclusion

Experiments with deposition of gypsum slurry layer with foam (at 0.19 wt%, and 1.86 wt% content) by a roller on a moving plastic belt were conducted. The roller could be either co-rotating with the belt, or non-rotating, as well as counter-rotating. The belt was non-wettable by water and slurry without foam, albeit it became partially wettable when a foaming agent was added. In a sense, the foaming agent facilitated spreading.

The maximum of the slurry-layer width measured on the roller was 4.36 times wider than the original layer width in the case with 1.86 wt% foam added and a co-rotating roller with a maximum rotation speed of 504 rpm. It was demonstrated that spreading of the slurry layer could be regulated by adding foam, rather than only controlling the roller rotation direction or its rotation speed. The layer width increased as more foam was added. As the foam content increased, the lateral widening of the deposited layer increased.

In the present viscosity-dominated flow of gypsum slurry entrained into a narrow gap under a roller by viscous stresses a significant pressure rise is expected as a direct consequence of the momentum balance equation, as predicted theoretically in the previous work of this group Plog and Yarin (2023). Accordingly, in the present situation of a flow unrestricted in the spanwise direction, such a pressure rise inevitably leads to gypsum slurry spreading on the substrate paper in the spanwise direction, as predicted in Ref. Plog and Yarin (2023), and experimentally demonstrated in the present work.

To ensure the reliability of the results, two different software programs (PIVlab and PIVware) were employed. Their results were in reasonable agreement despite some differences.

5 Competing interests

The authors declare no competing interests.

Supplementary Information The online version contains supplementary material available at https://doi.org/10.1007/s00348-025-04076-z.

Acknowledgements The authors are grateful for the support provided by the United States Gypsum.

Author contribution Y.I.K., D.P., and C.S. did the experiment, wrote the main manuscript text, and prepared figures J.W. provided the PIV software and analyzed the PIV results. A.L.Y. supervised the project, supplied the resources, and secured the funding as well as analyzed the results and wrote the manuscript. All authors reviewed the manuscript.

Data availability No datasets were generated or analysed during the current study.

References

Adrian R, Westerweel J (2011) Particle image velocimetry. Cambridge University Press, New York

Auernhammer GK, Fataei S, Haustein MA, Patel HP, Schwarze R, Secrieru E, Mechtcherine V (2020) Transparent model concrete with tunable rheology for investigating flow and particle-migration during transport in pipes. Mater des 193:108673

Bourne M (2002) Food texture and viscosity: concept and measurement. Elsevier, Amsterdam

Brazinsky I, Cosway H, Valle C Jr, Jones RC, Story V (1970) A theoretical study of liquid-film spread heights in the calendering of Newtonian and power law fluids. J Appl Polym Sci 14:2771–2784

Dannessa D, Sinha-Ray S, Jun S, Yarin AL (2018) Jets of three-phase power-law fluids and foam jet mixing in gypsum slurry. Constr Build Mater 166:922–944

Ivens U, Steinkjer B, Serup J, Tetens V (2001) Ointment is evenly spread on the skin, in contrast to creams and solutions. Br J Dermatol 145:264–267

Kim YI, Sanchez C, Podstawski D, Westerweel J, Yarin AL (2025) Spanwise spreading of gypsum slurry during deposition on the belt under a roller. J Appl Phys 137(22):224702

Kusakari K, Yoshida M, Matsuzaki F, Yanaki T, Fukui H, Date M (2003) Evaluation of post-application rheological changes in cosmetics using a novel measuring device: relationship to sensory evaluation. J Cosmet Sci 54:321–334

Le HD, Kadri EH, Aggoun S, Vierendeels J, Troch P (2015) Effect of lubrication layer on velocity profile of concrete in a pumping pipe. Mater Struct 48:3991–4003

Lee SJ, Kim GB, Yim DH, Jung SY (2009) Development of a compact x-ray particle image velocimetry for measuring opaque flows. Rev Sci Instrum 80:3

Li Y, Ren S (2011) Building decorative materials. Elsevier, Amsterdam

Liu C, Gao J, Tang Y, Chen X (2018) Preparation and characterization of gypsum-based materials used for 3D robocasting. J Mater Sci 53:16415–16422

Loeffel M, Ferguson SJ, Nolte L-P, Kowal JH (2008) Vertebroplasty: experimental characterization of polymethylmethacrylate bone cement spreading as a function of viscosity, bone porosity, and flow rate. Spine 33:1352–1359

Loitsyanskii LG (2014) Mechanics of liquids and gases. Elsevier, Amsterdam

Meinhart CD, Wereley ST, Santiago JG (2000) A PIV algorithm for estimating time-averaged velocity fields. J Fluids Eng 122:285–289

Pelot DD, Sahu RP, Sinha-Ray S, Yarin AL (2013) Strong squeeze flows of yield-stress fluids: the effect of normal deviatoric stresses. J Rheol 57(3):719–742

Pelot DD, Klep N, Yarin AL (2016) Spreading of carbopol gels. Rheol Acta 55:279–291

Plog J, Yarin AL (2023) Speed of sound in gypsum slurries with foaming agent and expected spanwise spreading. Exp Fluids 64:125

Poelma C (2020) Measurement in opaque flows: a review of measurement techniques for dispersed multiphase flows. Acta Mech 231(6):2089–2111

Raucci JS, Cecel RT, Romano RC, Pileggi RG, John VM (2018) Effect of mixing method on the mini-slump spread of Portland cement pastes. Rev IBRACON De Estruturas e Materiais. 11(02):410–431

Sadeghi M, Sontti SG, Zheng E, Zhang X (2023) Computational fluid dynamics (CFD) simulation of three–phase non–Newtonian slurry flows in industrial horizontal pipelines. Chem Eng Sci 270:118513

Sankaran A, Karakashev SI, Sett S, Grozev N, Yarin AL (2019) On the nature of the superspreaders. Adv Coll Interface Sci 263:1–18

Schlichting H (1979) Boundary layer theory. McGraw-Hill, New York

Sett S, Sahu RP, Pelot DD, Yarin AL (2014a) Enhanced foamability of sodium dodecyl sulfate mixed with superspreader trisiloxane-(poly)ethoxylate. Langmuir 30:14765–14775

Sett S, Sahu RP, Sinha-Ray S, Yarin AL (2014b) Superspreaders versus "cousin" non- superspreaders: disjoining pressure in gravitational film drainage. Langmuir 30:2619–2631

Sinha-Ray S, Srikar R, Lee CC, Li A, Yarin AL (2011) Shear and elongational rheology of gypsum slurries. Appl Rheol 21:63071

Turian RM, Ma TW, Hsu FLG, Sung DJ (1997) Characterization, settling, and rheology of concentrated fine particulate mineral slurries. Powder Technol 93(3):219–233

Xu B, Zhou S, He F, Wang F, Guo J (2020) Using particle image velocimetry to evaluate the displacement efficiency of drilling mud in horizontal well cementing. J Petrol Sci Eng 195:107647

Zhang P, Peterson SD, Porfiri M (2019) Combined particle image velocimetry/digital image correlation for load estimation. Exp Thermal Fluid Sci 100:207–221

Zheng H, Liu L, Williams L, Hertzberg JR, Lanning C, Shandas R (2006) Real time multicomponent echo particle image velocimetry technique for opaque flow imaging. Appl Phys Lett 88:26